

www.acsami.org Research Article

Aqueous Zn-Tetrazine Batteries with Cooperative Zn2+/H+ Insertion

Christopher Walter, Mark Yaseen, Jaehyun Park, Madison R. Tuttle, Sophia Taylor, and Shiyu Zhang*



Cite This: ACS Appl. Mater. Interfaces 2024, 16, 5937-5942



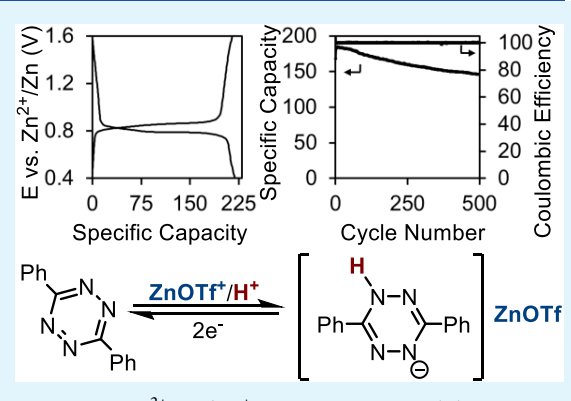
ACCESS I

Metrics & More

Article Recommendations

s Supporting Information

ABSTRACT: We present the investigation of 1,2,4,5-tetrazine derivatives as low-cost and synthetically modular organic electrode materials in rechargeable aqueous Zn-ion batteries (AZIBs). The substituents at the 3,6-positions of tetrazine were found to be critical for cycling stability. While heteroatom substituents (chloro, methoxy, and pyrazole) lead to the rapid decomposition of electrode materials in the electrolyte, the installation of phenyl groups enhances the cycling stability via π – π stacking. Spectroscopic characterization suggests a cooperative Zn²+ and H+ insertion mechanism. This unique cooperativity of Zn²+ and H+ leads to a steady discharge plateau in contrast to the undesirable sloping voltage profile typically observed in Zn-organic batteries.



KEYWORDS: aqueous zinc-ion battery, tetrazine, organic electrode materials, cooperative Zn²⁺ and H⁺ insertion, sustainability

■ INTRODUCTION

Aqueous zinc-ion batteries (AZIBs) are a class of promising grid-scale energy storage systems due to their inherent safety and low cost. The high theoretical capacity (820 mAh g⁻¹), stability, and low toxicity of zinc metal make it an ideal anode material for AZIBs.^{1,2} Conventional cathode materials in AZIBs are based on inorganic metal materials, e.g., manganese oxides,³ vanadium oxides,^{4,5} and Prussian blue analogues.^{6–8} However, supply chain issues and high costs associated with transition metals limit their adoption in grid-scale energy storage. As an alternative, organic electrode materials (OEMs) based on abundant elements, e.g., C, H, N, and S, could overcome these problems.^{2,9–11} Recently reported Zn/quinone batteries^{12–20} (Figure 1A) exhibit comparable performance to state-of-the-art Zn/MnO₂ and Zn/VO₂ batteries.

Due to the structural diversity of organic compounds, a wide range of redox mechanisms have been discovered, including Zn^{2+} insertion, H^+ insertion, and Zn^{2+}/H^+ coinsertion. $^{17-25}$ Among them, the most intriguing is Zn^{2+}/H^+ coinsertion, as coinsertion of H^+ with Zn^{2+} generally affords additional specific capacity. However, a disadvantage of Zn^{2+}/H^+ coinsertion is that it often leads to discharge profiles with multiple plateaus (Figure 1A) because of the distinct electrochemical kinetics of Zn^{2+} vs H^+ insertion. A sloping discharge profile means that the cell voltage falls progressively throughout the discharge cycle, which is undesirable for energy storage applications.

Herein, we report several 1,2,4,5-tetrazine derivatives that undergo cooperative Zn²⁺ and H⁺ coinsertion in one step in contrast to stepwise sequential Zn²⁺/H⁺ insertion in other OEMs. This unique ion-insertion mechanism affords a steady discharge plateau (Figure 1B), unlike the sloping discharge

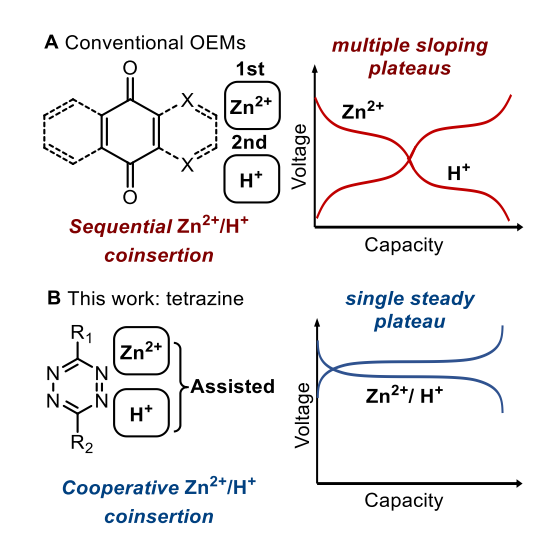


Figure 1. Comparison of sequential and cooperative $\mathrm{Zn^{2+}/H^{+}}$ coinsertion mechanisms and the representative voltage profiles of (A) OEMs in AZIBs with conventional quinone and/or imine-based motifs and (B) tetrazine cathode materials reported in this work.

profile in conventional OEMs. 17-19,21-24 Moreover, 1,2,4,5-tetrazines can be readily produced from gram-scale reactions of

Received: November 20, 2023 Revised: January 8, 2024 Accepted: January 8, 2024 Published: January 25, 2024





low-cost sulfur powder, hydrazine (N_2H_4), and organic nitriles. This stands in contrast to conventional OEMs, which typically require multiple synthetic steps and expensive reagents and suffer from poor scalability. Among the six tetrazine derivatives examined (Scheme 1), the best-performing compound 4 (3,6-

Scheme 1. Structure of Tetrazine Derivatives Investigated as Cathodes in AZIB in This Study

diphenyl-1,2,4,5-tetrazine) exhibits a specific capacity of 222 mAh $\rm g^{-1}$ at a stable voltage of 0.78 V in a Zn cell, giving rise to a specific energy of 173 Wh $\rm kg^{-1}$ that rivals the performance of start-of-the-art inorganic cathode materials in AZIBs.

MATERIALS AND METHODS

All experiments were carried out under a nitrogen (or argon) atmosphere using an MBraun glovebox and/or standard Schlenk techniques unless stated otherwise. ¹H and ¹³C NMR spectra were recorded on a Bruker 400 or 600 MHz spectrometer and were externally referenced to the NMR residual solvent peaks. ATR-IR spectra were measured using a Nicolet IR 200 with a diamond ATR accessory. Cyclic voltammetry and potentio-electrochemical impedance spectroscopy experiments were performed with a Biologic SP-150 or SP-50 single-channel potentiostat. Galvanostatic cycling experiments were performed with a LAND CT2001A battery testing system. X-ray fluorescence (XRF) spectra were measured by an Olympus/Innov-X X-5000 XRF analyzer with a tantalum X-ray tube source and a silicon drift detector. Unless otherwise noted, all solvents were degassed and dried using a Pure Process Technology (PPT) solvent purification system and stored under an atmosphere of nitrogen over 4 Å molecular sieves. All glassware were dried at 175 °C before use. All reagents were purchased from Sigma-Aldrich unless otherwise noted.

RESULTS

Solution and Solid-State Cyclic Voltammetry Study. Several tetrazines, including 3,6-bis(3,5-dimethylpyrazol-1-yl)-1,2,4,5-tetrazine (1), 3,6-dichloro-1,2,4,5-tetrazine (2), 3,6-dimethoxy-1,2,4,5-tetrazine (3), have been studied as anolytes in nonaqueous redox flow batteries and as cathodes in Li-ion batteries. Tetrazines typically exhibit a one-electron redox at ca. $-0.09~V~vs~Zn^{2+}/Zn$ (Figure 2A, red trace), rendering it impractical as cathode materials in AZIBs. However, the coordination of Lewis acidic ions, e.g., Sc^{3+} , Fe^{2+} , and Zn^{2+} , to tetrazine has been shown to shift their redox potentials anodically. $^{29-31}$

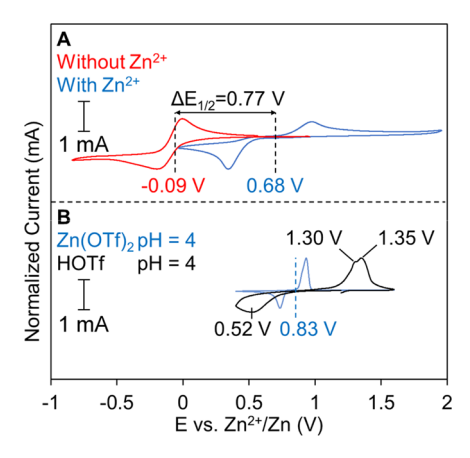


Figure 2. (A) Three-electrode solution CV of 4 with 0.1 M TBAClO $_4$ in MeCN (red) and 0.1 M TBAClO $_4$ + 0.01 M Zn(OTf) $_2$ in MeCN (blue) and (B) three-electrode solid-state CV of Zn-4 with 3 M Zn(OTf) $_2$ as the electrolyte (blue) and with pH 4 HOTf as the electrolyte (black).

To investigate the effect of Zn^{2+} on the redox potential of tetrazines under conditions relevant to AZIBs, we synthesized six derivatives 1-6 (Scheme 1). $^{28,32-36}$ The cyclic voltammogram (CV) of 4 in acetonitrile (MeCN) with 0.1 M tetrabutylammonium perchlorate (TBAClO₄) and 0.01 M zinc triflate (Zn(OTf)₂) shows a quasi-reversible redox event at 0.68 V vs Zn²⁺/Zn, representing a remarkable shift of 0.77 V upon Zn²⁺ addition (Figure 2A, blue trace). The solid-state CV of 4 in a two-electrode cell with 3 M Zn(OTf)₂ as an electrolyte shows a quasi-reversible redox process at 0.83 V vs Zn²⁺/Zn (Figure 2B, blue trace).

The redox event at 0.83 V could be attributed to the insertion of either Zn²⁺ or H⁺ due to the acidic nature of the electrolyte (pH 3.5–4.0).³⁷ To discern the insertion of H⁺ vs Zn²⁺, we measure the solid-state CV of 4 without Zn²⁺ at the same pH. A distinctly different CV profile was observed (Figure 2B, black trace). In the absence of Zn²⁺, compound 4 undergoes a two-electron two-proton insertion to form 4-H₂ (Scheme 1), a process that has a large voltage hysteresis (Figure S34). The significant voltage hysteresis in the 4/4-H₂ redox couple is likely attributed to substantial geometric rearrangements³⁸ and hydrogen bonding in the formation of 4-H₂.³⁹ In summary, the addition of Zn²⁺ decreases the charge—discharge gap and increases the redox potential; both are desirable outcomes for battery application.

Galvanostatic Cycling of Tetrazine Derivatives 1–6. The cycling performances of tetrazine derivatives 1–6 were investigated in two-electrode coin cells by using Zn metal as the anode and 3 M zinc sulfate (ZnSO₄) or Zn(OTf)₂ as the electrolyte. The galvanostatic charge–discharge (GCD) cycling experiments were performed at a rate of 1C assuming two-electron redox processes (200 mA g⁻¹ for 1, 356 mA g⁻¹ for 2, 284 mA g⁻¹ for 3, 229 mA g⁻¹ for 4, 311 mA g⁻¹ for 5, and 288 mA g⁻¹ for 6) with a voltage window of 0.4–1.6 V vs Zn²⁺/Zn. Coin cells of compounds 1, 2, and 3 show rapid capacity fading within the first 10 cycles (Figure S27–S29). The instability of 1–3 was attributed to their high solubility (Figures S41–S43), as coloration of the separator was observed (Figure S27B–S29B).

We sought to reduce the solubility of tetrazine in an aqueous environment by implementing $\pi - \pi$ stacking. ^{17,40–42} The structure of compound 4 in the solid state features extended

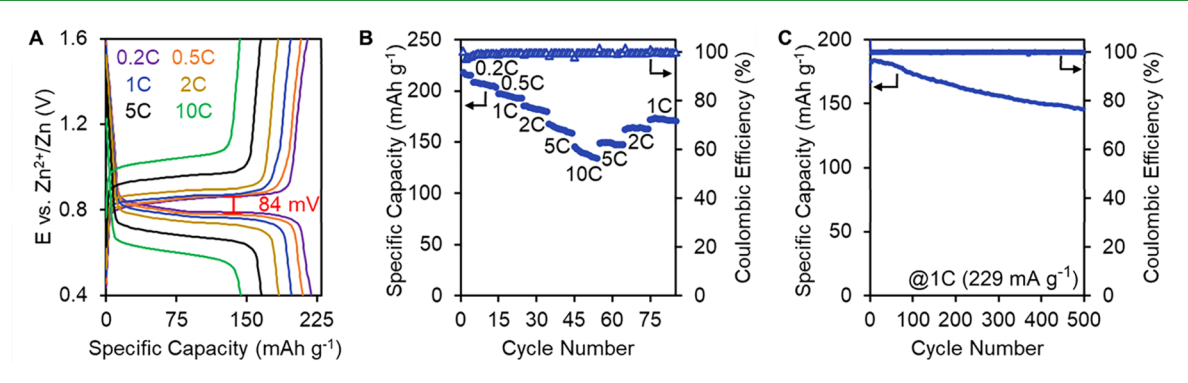


Figure 3. (A) Galvanostatic charge—discharge profile of Zn-4 cells, (B) variable-rate performance, and (C) long-term cycling stability at a rate of $1C (229 \text{ mA g}^{-1}).$

 π - π stacking (Figure S38), which is expected to prevent dissolution. Indeed, the GCD of Zn-4 cells exhibits a discharge capacity of 222 mAh g⁻¹, corresponding to 96.9% of the theoretical capacity (Figure 3A, purple). The GCD curve shows a flat discharge plateau at 0.78 V and a charge plateau at 0.86 V with a small voltage hysteresis of only 84 mV (Figure 3A). Variable-rate experiments conducted at 0.2C, 0.5C, 1C, 2C, 5C, and 10C of Zn-4 cells show capacities at 222, 210, 198, 187, 170, and 148 mAh g⁻¹, respectively (Figure 3B). Long-term cycling of compound 4 at 1C exhibits good stability with ca. 80% capacity retention after 500 cycles (Figure 3C). Post-mortem analysis of the cathode after 200 cycles shows buildup of the $Zn_x(OTf)_y(OH)_{2xy}*(H_2O)_n$ precipitate, which could contribute to the loss of capacity.

A Ragone plot of specific energy and power (specific energy and power based on the mass of active material of 4 in the cathode only) shows that compound 4 exhibits a performance similar to that of state-of-the-art inorganic cathode materials in AZIBs, e.g., MnO₂ and V₂O₅ (Figure 4, red trace). Despite

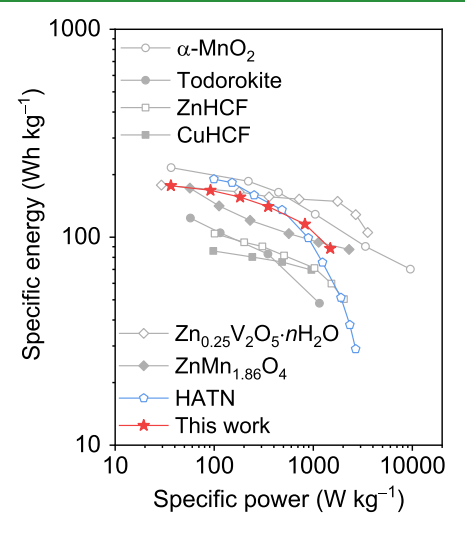


Figure 4. Ragone plot comparing the performance of 4 to state-ofthe-art inorganic and organic cathodes in AZIBs. 8,13,43-

having a slightly lower specific capacity (222 mAh g⁻¹), 4 shows comparable or superior specific energy than state-of-theart organic AZIB materials, such as HATN (418 mAh g⁻¹, Figure 4, blue trace).¹³ This was attributed to the stable discharge voltage of 4.

We also attempted to increase the specific capacity of 4 further by replacing one phenyl group with a methyl group in 5

or an ethyl group in 6. However, the removal of the phenyl group in 5 and 6 leads to a higher solubility (Figures S41-S43) and significantly faster capacity fading (Figures S30-S32).

Evidence for Zn²⁺ Insertion in 4. After demonstrating the cycling performance of 4 in AZIBs, we set out to investigate its redox mechanism that leads to a stable discharge profile. A galvanostatic intermittent titration technique study showed that 4 has a diffusion coefficient of $1.15 \times 10^{-11} \text{ m}^2$ s⁻¹, similar to typical diffusion rates for Zn²⁺ in organic cathodes (Figure S35). 17,48

X-ray fluorescence spectroscopic (XRF) analysis shows a significant increase of the Zn signal from 0 to 1796 counts/s upon discharge, followed by a significant decrease upon recharge (Figure 5B). This result, however, must be interpreted with care since the substantial variation in the Zn XRF signal can also be attributed to the formation of zinc hydroxide-based precipitation, such as $Zn_x(OTf)_v(OH)_{2x-v}$. (H₂O)_n, upon proton insertion. ^{7,20,49} Upon charging, the Zn signal was reduced to 112 counts/s. The small amount of the residual Zn signal is likely due to incomplete dissolution of $Zn_x(OTf)_v(OH)_{2x-v}y\cdot(H_2O)_n$ precipitation upon charging (vide infra, Figure \$22).

To address this ambiguity, we performed scanning electron microscopy (SEM) measurements and energy-dispersive X-ray spectroscopy (EDX) for elemental mapping. The discharge product of 4, as marked by N mapping, overlaid with elemental mapping of Zn and F, suggesting that it contains evenly distributed [Zn(OTf)]⁺ ions (Figure 6). This observation is consistent with the insertion of Zn²⁺ during discharge. Additionally, on the surface of the electrode, we found distinct flake-like crystals with strong Zn signals that can be attributed to $Zn_x(OTf)_y(OH)_{2x-y}y(H_2O)_n$ (Figure S21B). 7,20,49

Evidence for H⁺ Insertion in 4. After confirming the insertion of Zn²⁺, we considered if H⁺ insertion was playing a role in the redox of 4. Typically, Zn²⁺ and H⁺ coinsertion results in two-separate plateaus because of the distinct electrochemical kinetics of Zn²⁺ vs H⁺ insertion. ^{17–24} The stable discharge profile of 4 suggests that the coinsertion of Zn²⁺ and H⁺ is unlikely.

However, to our surprise, we found substantial evidence of H⁺ insertion. First, IR analysis of the discharged cathode powder shows a sharp peak at 3294 cm⁻¹ and a broad peak from 3300 to 3650 cm⁻¹ (Figure 5C). The sharp peak was assigned to the N-H stretch from the proton-inserted product. The broad peak was assigned to $Zn_x(OTf)_y(OH)_{2x-y}y\cdot (H_2O)_n$ a common product of H+ insertion due to the local basic environment created by H⁺ insertion. Upon charging, the N-

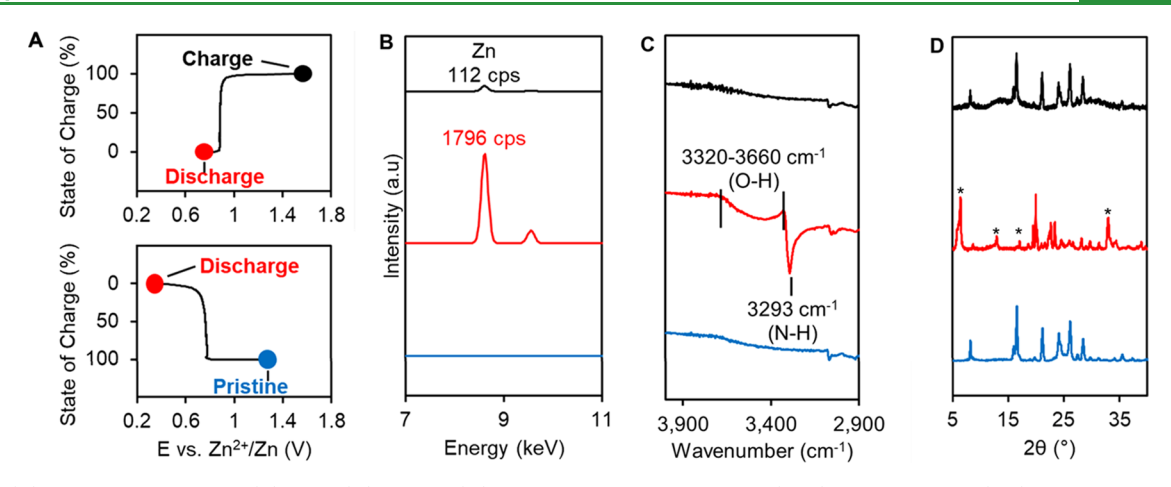


Figure 5. (A) GCD profile of 4 and (B) XRF, (C) IR, and (D) PXRD analysis of the pristine (blue), discharge state (red), and charge state (black) of cathode 4. The stars in the PXRD profile denote the features of $Zn_x(OTf)_v(OH)_{2x\sim v}y\cdot (H_2O)_n$.

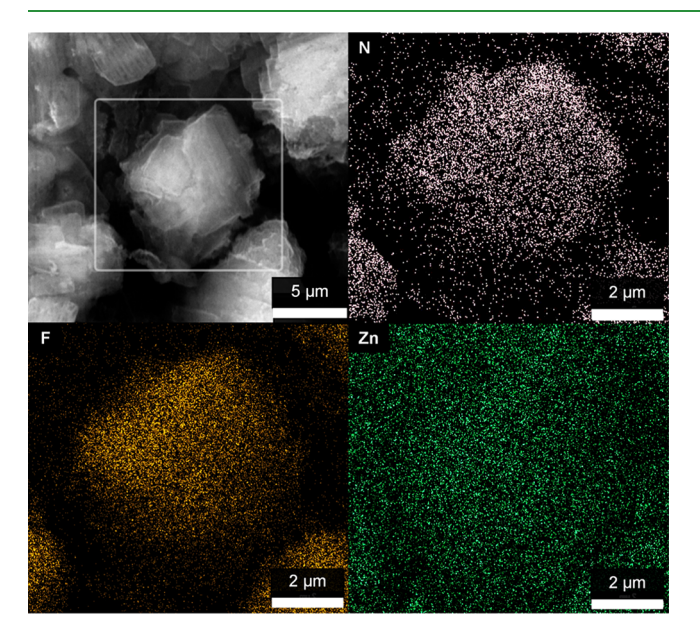


Figure 6. SEM image (top left) with corresponding EDX signal mapping of N (gray), F (yellow), and Zn (green) atoms for discharge state **4-Zn-H**.

H and the O–H vibrations both disappear, and the original IR profile for pristine 4 returns.

The formation of $Zn_x(OTf)_y(OH)_{2x-y}y\cdot(H_2O)_n$ is further supported by powder X-ray diffraction (PXRD) study. The PXRD pattern of the inorganic residues matches those reported for $Zn_x(OTf)_y(OH)_{2x-y}y\cdot(H_2O)_n$ (Figure 5D). The formation of zinc hydroxide precipitate is commonly attributed to H^+ insertion. These PXRD features disappear upon charging, suggesting that most of the $Zn_x(OTf)_y(OH)_{2x-y}y\cdot(H_2O)_n$ dissolves upon deinsertion of H^+ . Overall, both IR and PXRD studies confirmed the insertion of H^+ in 4.

Cooperativity of Zn^{2+} and H^+ Insertion in 4. Further examination of the PXRD data allows us to identify a PXRD pattern unique to the discharge product (Figure 5D). Importantly, these features do not match that of 4- H_2 (Figure S20), which is the discharge product of 4 under acidic conditions without Zn^{2+} . This intriguing observation indicates that the coinsertion of Zn^{2+} and H^+ into 4 does not yield distinct H^+ -insertion and Zn^{2+} -insertion products, in contrast

to previous studies. $^{17-24}$ Although we cannot entirely rule out the possibility of a different phase of 4-H₂, the cycling behavior of 4-H₂ is drastically different from that of 4 (Figure S34). This dissimilarity strongly suggests that 4-H₂ is not a discharge product of 4 within a Zn electrolyte environment.

Taken together, the most likely redox mechanism involves a two-electron, one-proton reduction of 4 to 4-Zn-H, which precipitates out as a triflate salt. The increase in pH in the local environment leads to the concurrent formation of $Zn_x(OTf)_y(OH)_{2x-y}y\cdot(H_2O)_n$ (Scheme 2). During charging,

Scheme 2. Proposed Mechanism for the Redox of 4 in AZIB

$$\begin{array}{c|ccccc} Ph & & +2e^{-} & & & & \\ N & N & & + ZnOTf^{+}/H^{+} & & & & Ph \\ N-N & & & & + ZnOTf^{+}/H^{+} & & \\ Ph & & & & + ZnOTf^{+}/H^{+} & \\ & & & & + Zn_{x}(OTf)_{y}(OH)_{2x-y}^{*}(H_{2}O)_{n} \end{array}$$

 Zn^{2+} and H^+ deinsert to restore the pristine crystalline structure of 4 and decrease the local pH, causing most of $Zn_x(OTf)_y(OH)_{2x-y}y\cdot(H_2O)_n$ to redissolve (Figure S22). This cooperative Zn^{2+}/H^+ insertion mechanism is consistent with the single stable discharge plateau observed in the GCD profile, in contrast to conventional Zn^{2+}/H^+ coinsertion materials, which often exhibit discharge profiles with multiple plateaus (Figure 1A) due to the distinct electrochemical kinetics of Zn^{2+} vs H^+ insertion.

CONCLUSIONS

In summary, we describe the electrochemical performance of low-cost tetrazine derivatives in AZIBs. The substituents on the 3,6-position of the tetrazine have a significant impact on the cycling stability in AZIBs. Installation of phenyl groups in 4 leads to decreased solubility, likely as a result of additional π – π stacking interactions. Compound 4 exhibits discharge at a capacity of 222 mAh g⁻¹ at a steady voltage of 0.78 V, giving rise to a specific energy comparable to that of the state-of-theart inorganic cathode materials in AZIBs.

Electrochemical and spectroscopic studies reveal a unique redox mechanism of 4 where Zn²⁺ and H⁺ insertion cooperatively occurs in one electrochemical step to generate

a single discharge product. Our work highlights that cooperative insertion of $\mathrm{Zn^{2+}}$ and $\mathrm{H^{+}}$ produces a stable discharge plateau, in contrast to the sloping discharge profile typically seen in $\mathrm{Zn^{2+}}$ and $\mathrm{H^{+}}$ coinsertion materials. We anticipate that cooperative $\mathrm{Zn^{2+}}/\mathrm{H^{+}}$ insertion mechanism will be observed in a broader range of redox-active organic materials in AZIBs. 14,53 Cooperative insertion of $\mathrm{Zn^{2+}}/\mathrm{H^{+}}$ should be considered as a strategy for designing OEMs with stable discharge voltage profiles.

ASSOCIATED CONTENT

Supporting Information

The Supporting Information is available free of charge at https://pubs.acs.org/doi/10.1021/acsami.3c17412.

Experimental procedures, synthesis and characterization, XRD measurements, electrochemical measurements, and battery testing (PDF)

AUTHOR INFORMATION

Corresponding Author

Shiyu Zhang — Department of Chemistry & Biochemistry, The Ohio State University, Columbus, Ohio 43210, United States; orcid.org/0000-0002-2536-4324; Email: zhang.8941@osu.edu

Authors

Christopher Walter – Department of Chemistry & Biochemistry, The Ohio State University, Columbus, Ohio 43210, United States

Mark Yaseen — Department of Chemistry & Biochemistry, The Ohio State University, Columbus, Ohio 43210, United States

Jaehyun Park – Department of Chemistry & Biochemistry, The Ohio State University, Columbus, Ohio 43210, United

Madison R. Tuttle – Department of Chemistry & Biochemistry, The Ohio State University, Columbus, Ohio 43210, United States

Sophia Taylor – Department of Chemistry & Biochemistry, The Ohio State University, Columbus, Ohio 43210, United States

Complete contact information is available at: https://pubs.acs.org/10.1021/acsami.3c17412

Notes

The authors declare no competing financial interest.

ACKNOWLEDGMENTS

This work was supported by the National Science Foundation under CBET-2124604, the Sustainability Institute at Ohio State University, and the Center for Emergent Materials, NSF MRSEC, under award number DMR-2011876.

REFERENCES

- (1) Song, M.; Tan, H.; Chao, D.; Fan, H. J. Recent Advances in Zn-Ion Batteries. *Adv. Funct. Mater.* **2018**, 28, No. 1802564.
- (2) Zhang, N.; Chen, X.; Yu, M.; Niu, Z.; Cheng, F.; Chen, J. Materials Chemistry for Rechargeable Zinc-Ion Batteries. *Chem. Soc. Rev.* 2020, 49, 4203–4219.
- (3) Sun, W.; Wang, F.; Hou, S.; Yang, C.; Fan, X.; Ma, Z.; Gao, T.; Han, F.; Hu, R.; Zhu, M.; Wang, C. Zn/MnO₂ Battery Chemistry With H⁺ and Zn²⁺ Coinsertion. *J. Am. Chem. Soc.* **2017**, *139*, 9775–9778.

- (4) Ding, J.; Du, Z.; Li, B.; Wang, L.; Wang, S.; Gong, Y.; Yang, S. Unlocking the Potential of Disordered Rocksalts for Aqueous Zinc-Ion Batteries. *Adv. Mater.* **2019**, *31*, 1904369.
- (5) Wan, F.; Zhang, L.; Dai, X.; Wang, X.; Niu, Z.; Chen, J. Aqueous Rechargeable Zinc/Sodium Vanadate Batteries with Enhanced Performance from Simultaneous Insertion of Dual Carriers. *Nat. Commun.* **2018**, *9*, No. 1656.
- (6) Godeffroy, L.; Aguilar, I.; Médard, J.; Larcher, D.; Tarascon, J. M.; Kanoufi, F. Decoupling the Dynamics of Zinc Hydroxide Sulfate Precipitation/Dissolution in Aqueous Zn-MnO₂ Batteries by Operando Optical Microscopy: A Missing Piece of the Mechanistic Puzzle. Adv. Energy Mater. 2022, 12, 2200722.
- (7) Wang, L.; Huang, K. W.; Chen, J.; Zheng, J. Ultralong Cycle Stability of Aqueous Zinc-Ion Batteries with Zinc Vanadium Oxide Cathodes. *Sci. Adv.* **2019**, *5*, eaax4279.
- (8) Zhang, L.; Chen, L.; Zhou, X.; Liu, Z. Towards High-Voltage Aqueous Metal-Ion Batteries Beyond 1.5 V: The Zinc/Zinc Hexacyanoferrate System. *Adv. Energy Mater.* **2015**, *5*, No. 1400930.
- (9) Wang, H.-g.; Wu, Q.; Cheng, L.; Zhu, G. The Emerging Aqueous Zinc-Organic Battery. *Coord. Chem. Rev.* **2022**, 472, No. 214772.
- (10) Deng, X.; Sarpong, J. K.; Zhang, G.; Hao, J.; Zhao, X.; Li, L.; Li, H.; Han, C.; Li, B. Proton Storage Chemistry in Aqueous Zinc-Organic Batteries: A Review. *InfoMat* **2023**, *5*, e12382.
- (11) Lu, Y.; Zhang, Q.; Li, L.; Niu, Z.; Chen, J. Design Strategies toward Enhancing the Performance of Organic Electrode Materials in Metal-Ion Batteries. *Chem* **2018**, *4*, 2786–2813.
- (12) Chen, Y.; Dai, H.; Fan, K.; Zhang, G.; Tang, M.; Gao, Y.; Wang, C. A Recyclable and Scalable High-Capacity Organic Battery. *Angew. Chem.* **2023**, No. e202302539.
- (13) Chen, Y.; Li, J.; Zhu, Q.; Fan, K.; Cao, Y.; Zhang, G.; Zhang, C.; Gao, Y.; Zou, J.; Zhai, T.; et al. Two-Dimensional Organic Supramolecule via Hydrogen Bonding and $\pi-\pi$ Stacking for Ultrahigh Capacity and Long-Life Aqueous Zinc-Organic Batteries. *Angew. Chem., Int. Ed.* **2022**, *61*, No. e202116289.
- (14) Wang, Y.; Wang, C.; Ni, Z.; Gu, Y.; Wang, B.; Guo, Z.; Wang, Z.; Bin, D.; Ma, J.; Wang, Y. Binding Zinc Ions by Carboxyl Groups from Adjacent Molecules toward Long-Life Aqueous Zinc-Organic Batteries. *Adv. Mater.* **2020**, *32*, No. 2000338.
- (15) Guo, Z.; Ma, Y.; Dong, X.; Huang, J.; Wang, Y.; Xia, Y. An Environmentally Friendly and Flexible Aqueous Zinc Battery Using an Organic Cathode. *Angew. Chem., Int. Ed.* **2018**, *57*, 11737–11741.
- (16) Sun, T.; Li, Z. J.; Zhi, Y. F.; Huang, Y. J.; Fan, H. J.; Zhang, Q. Poly(2,5-Dihydroxy-1,4-Benzoquinonyl Sulfide) As an Efficient Cathode for High-Performance Aqueous Zinc—Organic Batteries. *Adv. Funct. Mater.* **2021**, *31*, No. 2010049.
- (17) Tie, Z.; Zhang, Y.; Zhu, J.; Bi, S.; Niu, Z. An Air-Rechargeable Zn/Organic Battery with Proton Storage. *J. Am. Chem. Soc.* **2022**, *144*, 10301–10308.
- (18) Tie, Z.; Liu, L.; Deng, S.; Zhao, D.; Niu, Z. Proton Insertion Chemistry of a Zinc-Organic Battery. *Angew. Chem., Int. Ed.* **2020**, 59, 4920–4924.
- (19) Wan, F.; Zhang, L.; Wang, X.; Bi, S.; Niu, Z.; Chen, J. An Aqueous Rechargeable Zinc-Organic Battery with Hybrid Mechanism. *Adv. Funct. Mater.* **2018**, 28, No. 1804975.
- (20) Zhao, Q.; Huang, W.; Luo, Z.; Liu, L.; Lu, Y.; Li, Y.; Li, L.; Hu, J.; Ma, H.; Chen, J. High-Capacity Aqueous Zinc Batteries Using Sustainable Quinone Electrodes. *Sci. Adv.* **2018**, *4*, No. eaao1761.
- (21) Na, M.; Oh, Y.; Byon, H. R. Effects of Zn²⁺ and H⁺ Association with Naphthalene Diimide Electrodes for Aqueous Zn-Ion Batteries. *Chem. Mater.* **2020**, 32, 6990–6997.
- (22) Wang, Y.; Wang, X.; Tang, J.; Tang, W. A Quinoxalinophenazinedione Covalent Triazine Framework for Boosted High-Performance Aqueous Zinc-Ion Batteries. *J. Mater. Chem. A* **2022**, 10, 13868–13875.
- (23) Gao, Y.; Li, G.; Wang, F.; Chu, J.; Yu, P.; Wang, B.; Zhan, H.; Song, Z. A High-Performance Aqueous Rechargeable Zinc Battery Based on Organic Cathode Integrating Quinone and Pyrazine. *Energy Storage Mater.* **2021**, *40*, 31–40.

- (24) Tuttle, M. R.; Walter, C.; Brackman, E.; Moore, C. E.; Espe, M.; Rasik, C.; Adams, P.; Zhang, S. Redox-Active Zinc Thiolates for Low-Cost Aqueous Rechargeable Zn-Ion Batteries. *Chem. Sci.* **2021**, 12, 15253–15262.
- (25) Li, W.; Xu, H.; Zhang, H.; Wei, F.; Huang, L.; Ke, S.; Fu, J.; Jing, C.; Cheng, J.; Liu, S. Tuning Electron Delocalization of Hydrogen-Bonded Organic Framework Cathode for High-Performance Zinc-Organic Batteries. *Nat. Commun.* **2023**, *14*, No. 5235.
- (26) De La Garza, G. D.; Kaur, A. P.; Shkrob, I. A.; Robertson, L. A.; Odom, S. A.; McNeil, A. J. Soluble and Stable Symmetric Tetrazines as Anolytes in Redox Flow Batteries. *J. Mater. Chem. A* **2022**, *10*, 18745–18752.
- (27) Min, D. J.; Lee, K.; Park, H.; Kwon, J. E.; Park, S. Y. Redox Potential Tuning of S-Tetrazine by Substitution of Electron-Withdrawing/Donating Groups for Organic Electrode Materials. *Molecules* **2021**, *26*, 894.
- (28) Min, D. J.; Miomandre, F.; Audebert, P.; Kwon, J. E.; Park, S. Y. S-Tetrazines as a New Electrode-Active Material for Secondary Batteries. *ChemSusChem* **2019**, *12*, 503–510.
- (29) Beagan, D. M.; Maciulis, N. A.; Pink, M.; Carta, V.; Huerfano, I. J.; Chen, C. H.; Caulton, K. G. A Redox-Active Tetrazine-Based Pincer Ligand for the Reduction of N-Oxyanions Using a Redox-Inert Metal. *Chem. A Eur. J.* **2021**, *27*, 11676—11681.
- (30) Benson, C. R.; Hui, A. K.; Parimal, K.; Cook, B. J.; Chen, C. H.; Lord, R. L.; Flood, A. H.; Caulton, K. G. Multiplying the Electron Storage Capacity of a Bis-Tetrazine Pincer Ligand. *Dalton Trans.* **2014**, *43*, 6513–6524.
- (31) Fukuzumi, S.; Yuasa, J.; Suenobu, T. Scandium Ion-Promoted Reduction of Heterocyclic N = N Double Bond. Hydride Transfer vs Electron Transfer. *J. Am. Chem. Soc.* **2002**, *124*, 12566–12573.
- (32) Alfaruqi, M. H.; Mathew, V.; Gim, J.; Kim, S.; Song, J.; Baboo, J. P.; Choi, S. H.; Kim, J. Electrochemically Induced Structural Transformation in a γ -MnO $_2$ Cathode of a High Capacity Zinc-Ion Battery System. *Chem. Mater.* **2015**, *27*, 3609–3620.
- (33) Nhu, D.; Duffy, S.; Avery, V. M.; Hughes, A.; Baell, J. B. Antimalarial 3-Arylamino-6-Benzylamino-1,2,4,5-Tetrazines. *Bioorg. Med. Chem. Lett.* **2010**, *20*, 4496–4498.
- (34) Chavez, D. E.; Hiskey, M. Synthesis of the Bi-Heterocyclic Parent Ring System 1,2,4-Triazolo[4,3-b][1,2,4,5]Tetrazine and Some 3,6-Disubstituted Derivatives. *J. Heterocycl. Chem.* **1998**, 35, 1329–1332.
- (35) Chen, D.; Yang, H.; Yi, Z.; Xiong, H.; Zhang, L.; Zhu, S.; Cheng, G. $C_8N_{26}H_4$: An Environmentally Friendly Primary Explosive with High Heat of Formation. *Angew. Chem., Int. Ed.* **2018**, *57*, 2081–2084
- (36) Haddadin, M. J.; Zadeh, E. H. G. A Novel Method for the Synthesis of 3, 5-Disubstituted-(NH)-1,2,4-Triazoles. *Tetrahedron Lett.* **2010**, *51*, 1654–1656.
- (37) Zhao, X.; Zhang, X.; Dong, N.; Yan, M.; Zhang, F.; Mochizuki, K.; Pan, H. Advanced Buffering Acidic Aqueous Electrolytes for Ultra-Long Life Aqueous Zinc-Ion Batteries. *Small* **2022**, *18*, 2200742.
- (38) Polezhaev, A. V.; Maciulis, N. A.; Chen, C.; Pink, M.; Lord, R. L.; Caulton, K. G. Tetrazine Assists Reduction of Water by Phosphines: Application in the Mitsunobu Reaction. *Chem.—Eur. J.* **2016**, *22*, 13985–13998.
- (39) Ge, Y.; Miller, L.; Ouimet, T.; Smith, D. K. Electrochemically Controlled Hydrogen Bonding. O-Quinones as Simple Redox-Dependent Receptors for Arylureas. *J. Org. Chem.* **2000**, *65*, 8831–8838.
- (40) Murata, T.; Morita, Y.; Yakiyama, Y.; Fukui, K.; Yamochi, H.; Saito, G.; Nakasuji, K. Hydrogen-Bond Interaction in Organic Conductors: Redox Activation, Molecular Recognition, Structural Regulation, and Proton Transfer in Donor Acceptor Charge-Transfer Complexes of TTF-Imidazole. J. Am. Chem. Soc. 2007, 129, 10837—10846.
- (41) Tuttle, M. R.; Davis, S. T.; Zhang, S. Synergistic Effect of Hydrogen Bonding and $\pi \pi$ Stacking Enables Long Cycle Life in Organic Electrode Materials. *ACS Energy Lett.* **2021**, *6*, 643–649.

- (42) Peng, H.; Xiao, J.; Wu, Z.; Zhang, L.; Geng, Y.; Xin, W.; Li, J.; Yan, Z.; Zhang, K.; Zhu, Z. N-Heterocycles Extended π-Conjugation Enables Ultrahigh Capacity, Long-Lived, and Fast-Charging Organic Cathodes for Aqueous Zinc Batteries. CCS Chem. 2023, 5, 1789–1801.
- (43) Trócoli, R.; La Mantia, F. An Aqueous Zinc-Ion Battery Based on Copper Hexacyanoferrate. *ChemSusChem* **2015**, *8*, 481–485.
- (44) Lee, J.; Ju, J. B.; Cho, W. Il.; Cho, B. W.; Oh, S. H. Todorokite-Type MnO2 as a Zinc-Ion Intercalating Material. *Electrochim. Acta* **2013**, *112*, 138–143.
- (45) Kundu, D.; Adams, B. D.; Duffort, V.; Vajargah, S. H.; Nazar, L. F. A High-Capacity and Long-Life Aqueous Rechargeable Zinc Battery Using a Metal Oxide Intercalation Cathode. *Nat. Energy* **2016**, *1*, 16119.
- (46) Xu, C.; Li, B.; Du, H.; Kang, F. Energetic Zinc Ion Chemistry: The Rechargeable Zinc Ion Battery. *Angew. Chem., Int. Ed.* **2012**, *51*, 933–935.
- (47) Zhang, N.; Cheng, F.; Liu, Y.; Zhao, Q.; Lei, K.; Chen, C.; Liu, X.; Chen, J. Cation-Deficient Spinel ZnMn2O4 Cathode in Zn(CF3SO3)2 Electrolyte for Rechargeable Aqueous Zn-Ion Battery. *J. Am. Chem. Soc.* **2016**, *138*, 12894–12901.
- (48) Pan, Q.; Dong, R.; Lv, H.; Sun, X.; Song, Y.; Liu, X. X. Fundamental Understanding of the Proton and Zinc Storage in Vanadium Oxide for Aqueous Zinc-Ion Batteries. *Chem. Eng. J.* **2021**, *419*, No. 129491.
- (49) Oberholzer, P.; Tervoort, E.; Bouzid, A.; Pasquarello, A.; Kundu, D. Oxide versus Nonoxide Cathode Materials for Aqueous Zn Batteries: An Insight into the Charge Storage Mechanism and Consequences Thereof. ACS Appl. Mater. Interfaces 2019, 11, 674–682.
- (50) Dong, Y.; Miao, L.; Ma, G.; Di, S.; Wang, Y.; Wang, L.; Xu, J.; Zhang, N. Non-Concentrated Aqueous Electrolytes with Organic Solvent Additives for Stable Zinc Batteries. *Chem. Sci.* **2021**, *12*, 5843–5852.
- (51) Chen, L.; Yang, Z.; Wu, J.; Chen, H.; Meng, J. Energy Storage Performance and Mechanism of the Novel Copper Pyrovanadate Cu₃V₂O₇(OH)₂·2H₂O Cathode for Aqueous Zinc Ion Batteries. *Electrochim. Acta* **2020**, 330, No. 135347.
- (52) Chen, X.; Li, W. W.; Xu, Y.; Zeng, Z.; Tian, H.; Velayutham, M.; Shi, W.; Li, W. W.; Wang, C.; Reed, D.; et al. Charging Activation and Desulfurization of MnS Unlock the Active Sites and Electrochemical Reactivity for Zn-Ion Batteries. *Nano Energy* **2020**, *75*, No. 104869.
- (53) Kundu, D.; Oberholzer, P.; Glaros, C.; Bouzid, A.; Tervoort, E.; Pasquarello, A.; Niederberger, M. Organic Cathode for Aqueous Zn-Ion Batteries: Taming a Unique Phase Evolution toward Stable Electrochemical Cycling. *Chem. Mater.* **2018**, *30*, 3874–3881.